A New Route To Stabilize the Smectic C Phase in a Series of Laterally Attached Side-Chain Liquid Crystalline Polynorbornenes with a One-Carbon Spacer

Gue-Hyun Kim, Coleen Pugh,* and Stephen Z. D. Cheng*

Maurice Morton Institute and Department of Polymer Science, The University of Akron, Akron, Ohio 44325-3909

Received November 3, 1999; Revised Manuscript Received August 29, 2000

ABSTRACT: A series of polynorbornenes (PNBEs) with 1,4-bis[(3′-fluoro-4′-*n*-alkoxyphenyl)ethynyl]-benzene mesogens ($n = 9-12$) laterally attached to the polymer backbone through a one-carbon spacer were previously synthesized by ring-opening metathesis polymerization of the corresponding norbornene-based monomers. Wide-angle X-ray diffraction (WAXD) experiments demonstrate that the mesogens organize into the tilted layer structure of a smectic C (S_C) phase at room temperature, and polarized light microscopy demonstrates that the highest temperature ordered phase is a nematic (N) phase. Upon heating above room temperature, the tilt angle of the S_C phase of all of the PNBEs ($n = 9-12$) continuously decreases, especially at temperatures above 70 °C for the PNBEs ($n = 9-11$) and 60 °C for the PNBE ($n = 12$). However, the S_C phase of the PNBEs ($n = 9-11$) transforms to a N phase before the tilt angle reaches zero. That is, the S_A phase is never actually achieved in the PNBEs ($n = 9-11$), although the decrease in the tilt angles corresponds to a broad endotherm in the differential scanning calorimetry (DSC) experiments in the same temperature region. This speculation is proven by the stable S_A phase of PNBE ($n = 12$) observed by WAXD at temperatures above 83 °C. The transition between the S_C and S_A phases is not a first-order transition according to DSC measurements and is instead a second-order transition based on the gradual decrease to 0° in the tilt angle, which serves as an order parameter.

Introduction

Traditional side-chain liquid crystalline (LC) polymers are synthesized with the intention of retaining the LC behavior of low molecular mass liquid crystals, while trying to improve their mechanical and phase stability. The typical molecular design attaches the mesogens terminally to the polymer backbone. One disadvantage of using side-chain LC polymers for electrooptical display applications is their relatively high viscosity, which slows their response toward external fields.[1] Recently, interest in LCs that generate a smectic C (S_C) phase has increased because these molecules can be either functionalized with a chiral substituent or doped with chiral compounds to generate a S_C* phase, which spontaneously polarizes if the helix is unwound.[2] This decreases the switching time from one anisotropic orientation to the opposite orientation in side-chain LC polymers.

Although many terminally attached side-chain LC polymers have exhibited the S_C phase,[5] we[1,4] proposed that a more appropriate design for LC polymers that exhibit S_C phase behavior is to laterally attach extended mesogens to the polymer backbone. This is because low molecular mass liquid crystals tend to exhibit the S_C phase when they are based on symmetrically disubstituted extended mesogens with long *n*-alkoxy substituents,[3] and lateral attachment maintains the symmetric disubstitution of the extended mesogens. However, almost all laterally attached side-chain LC polymers synthesized so far have exhibited only the nematic (N) phase.[6−17] Since the laterally attached mesogens are generally much larger in size than the repeat units of the polymer backbone, the mesogens force the backbone into a somewhat extended helical conformation, thereby allowing the mesogens in the side chains to wrap around it to form a cylindrical mesogen jacket.[8,13,15,17] In this case, it should be difficult to form a smectic phase. Nevertheless, side-chain LC polymers with laterally attached 1,4-bis[(4′-*n*-alkoxybenzoyl)oxy]benzene mesogens can be forced to order into S_C layers by terminating their *n*-alkoxy substituents with either immiscible fluorocarbon[18] or siloxane[19] segments.

However, the question still remains whether laterally attached side-chain LC polymers can exhibit S_C phase behavior without introducing immiscible components. For example, laterally attached side-chain LC polynorbornenes (PNBEs) with symmetrically disubstituted extended mesogens and an 11-carbon spacer apparently exhibit only a N phase,[20] although the corresponding low molecular mass 1,4-bis[(3′-fluoro-4′-*n*-alkoxyphenyl)-ethynyl]benzenes with $n = 6-12$ exhibit a stable S_C phase over a relatively wide temperature range.[21,22] This is also in spite of the fact that long spacers generally favor smectic mesophases in terminally attached side-chain LC polymers.[23] Therefore, the lateral polymeric substituent apparently destabilizes the S_C phase.

To determine the extent to which lateral attachment destabilizes the S_C phase, this study investigates the phase behavior of a series of polynorbornenes (PNBEs)[22] with 1,4-bis[(3′-fluoro-4′-*n*-alkoxyphenyl)ethynyl]benzene mesogens ($n = 9-12$) laterally attached to the polymer backbone through a one-carbon spacer. Since the S_C phase is generally stabilized by increasing the number of methylenic units in the flexible substituents,[23] the effect of the lateral attachment may vary with the length of the *n*-alkoxy substituents. In addition to the glass transition, these polymers were previously reported to exhibit only a N phase during the time scale of a DSC experiment.[22]

* To whom correspondence should be addressed.

10.1021/ma9918607 CCC: $19.00
Published on Web 11/10/2000

Experimental Section

Materials. The series of PNBEs (n = 9−12) with approximately 50 repeat units and narrow polydispersity (pdi = 1.09−1.29) was synthesized by ring-opening metathesis polymerization of the corresponding 5-{[[2′,5′-bis[2-(3′-fluoro-4′-*n*-alkoxyphenyl)ethynyl]benzyl]oxy]carbonyl}bicyclo[2.2.1]hept-2-enes in THF using $Mo(CHCMe_2Ph)(N\text{-}2,6\text{-}^iPr_2Ph)(O^tBu)_2$ as the initiator. The detailed synthesis is reported in an earlier publication.[22] In brief, the monomers were synthesized by coupling 5-{[(2′,5′-diiodobenzyl)oxy]carbonyl}bicyclo[2.2.1]hept-2-ene with 2 equiv of a preformed 3-fluoro-4-*n*-alkoxyphenylacetylene using a catalytic amount of cuprous iodide in the presence of triphenylphosphine. The chemical structure of these PNBEs (n = 9−12) is shown below.

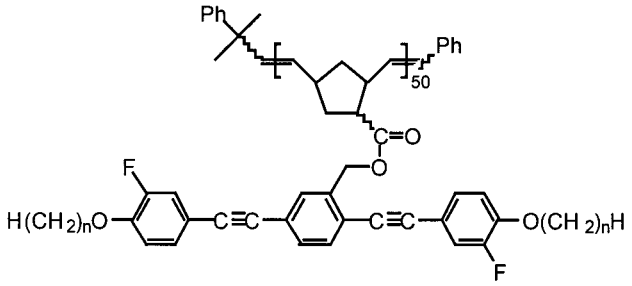

The number-average molecular weights of PNBEs (n = 9−12) were determined via gel permeation chromatography (GPC) based on polystyrene standards, and they are 5.42×10^4, 3.02×10^4, 3.86×10^4, and 4.55×10^4 g/mol, respectively, and their molecular weight distributions are 1.10, 1.09, 1.17, and 1.29, respectivly.[22]

Instrument and Experiments. The thermal transitions of the polymers were detected via a Perkin-Elmer DSC-7 instrument. The temperature and heat flow at different cooling and heating rates (0.5−20 °C/min) were calibrated using standard materials (benzoic acid, indium, and anisic acid). A typical DSC sample size was 1−2 mg. Cooling experiments were always conducted prior to each heating experiment, and the cooling and heating rates were identical. The transition temperatures were determined by measuring the onset and peak temperatures from the cooling and heating scans at different rates. Overlapped endothermic or exothermic peaks were resolved using the PeakFit peak separation program (Jandel Scientific). A Pearson IV (a_3 = 2) function was used to obtain the best fit based on our experience with this program.

Wide-angle X-ray diffraction (WAXD) powder experiments were performed with a Rigaku 12 kW rotating anode generator (Cu Kα radiation) equipped with a diffractometer. A hot stage was coupled with the diffractometer to study the structural evolution with temperature at constant heating and cooling rates. The temperature was controlled to better than ±0.5 °C. Films having a thickness of approximately 0.1 mm were mounted on aluminum sheets, and the diffraction patterns were collected in reflection mode. Samples were scanned in a 2θ range between 1.5° and 30°. Background scattering was subtracted from the sample diffraction patterns. To determine the correlation length of different phases, the widths at half-height (WAHH) of the low-angle reflections were also measured with increasing temperature.

Polarized FT-IR experiments of sheared films were conducted on a Mattson Galaxy series FT-IR 5000 spectrometer equipped with a helium:neon laser source and a polarizer rotation stage in a transmission geometry. The wavenumber accuracy was ±2 cm^{-1}. A rotation stage was used to control the tilt angle of the polarized IR beam with respect to the sample orientation. The rotating range was between 0° and 90° with an angular accuracy of ±0.5° in the azimuthal direction. The sample was uniaxially sheared in the liquid crystal phase on a KBr substrate using a mechanical force.

Fibers were spun from the liquid crystalline phase in order to determine phase structures. A typical fiber diameter was 30 μm. WAXD fiber patterns were obtained from a Rigaku Automated X-ray Imaging System (3000 × 3000 pixel resolution) with an 18 kW rotating anode X-ray generator. A hot stage was coupled with the diffractometer to study the structural evolution with temperature. A 50 min exposure was required for high-quality WAXD fiber patterns. The background scattering was again subtracted from the fiber patterns.

Phase morphology and liquid crystalline defects were examined via a polarized light microscope (PLM) (Olympus BH-2) coupled with a Mettler hot stage (FP-90). Both isothermal and nonisothermal experiments were performed for PLM observation, and film samples with a typical thickness of 10 μm were obtained by melt-pressing small amounts of samples between two glass slides.

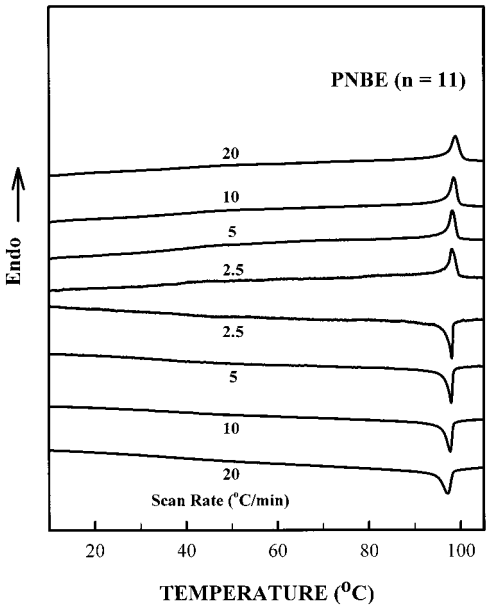

Figure 1. Two sets of DSC thermodiagrams of PNBE (n = 11) at different heating and cooling rates (2.5−20 °C/min).

Results and Discussion

Thermal Behavior of PNBEs(*n*). Figure 1 shows two sets of DSC cooling and subsequent heating thermal diagrams at different rates (2.5−20 °C/min) using PNBE (n = 11) as an example. As previously reported,[22] the glass transition temperature (T_g) occurs at around 40 °C in both heating and cooling experiments. An apparent first-order transition occurs at around 98 °C during cooling. The extent of supercooling depends little on the cooling rate, which confirms that the first-order transition involves a LC phase, and implies that the transitions are close to thermodynamic equilibrium.

However, the first-order transition has a higher onset transition temperature during cooling (98 °C) than on heating (97 °C), which may indicate an overlapped transition and/or a biphasic phenomenon. Careful examination of the DSC heating diagrams also indicates that a broad thermal event takes place before the major endothermic peak. This is supported by the lower heat capacity in the isotropic melt than at temperatures between 70 and 97 °C. If this broad transition is associated with structural changes in the LC phase(s), it must be either a weak first-order or a second-order transition. Furthermore, two transition processes are visible at very slow heating rates for these PNBEs. Figure 2 shows a DSC heating curve of PNBE (n = 11) at a heating rate of 0.5 °C/min. As confirmed by the WAXD experiments described in subsequent sections,

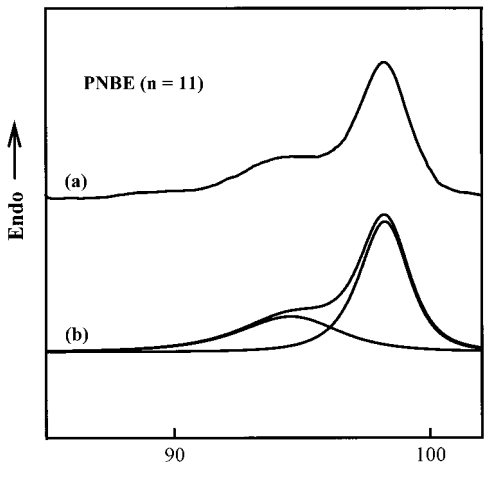

Figure 2. DSC thermodiagram of PNBE (n = 11) (a) at a heating rate of 0.5 °C/min, and (b) after peak separations.

Table 1. Transition Properties of PNBEs (n = 9−12) at a Heating Rate of 2.5 °C/min

n	T_{Sc-N} (°C)	ΔH_{Sc-N} (kJ/mol)	T_{N-I} (°C)	ΔH_{N-I} (kJ/mol)
9	97	0.9	101	1.9
10	96	1.0	99	2.0
11	95	1.3	98	2.2
12	87[a]	0.8[a]	91	2.3

[a] This temperature and heat of transition represent a S_A to N phase transition. The S_C to S_A transition in this PNBE (n = 12) is a second-order transition, and thus, no latent heat is involved.

these polymers therefore exhibit *three* thermal events. For PNBE (n = 11), for example, a broad transition starts at 70 °C, and two overlapped transitions appear at around 95 and at 98 °C. We have reported similar overlapped LC transitions in a series of main-chain/side-chain LC polyesters.[24]

The other PNBEs reported here exhibit similar DSC thermodiagrams. Their detailed transition properties are listed in Table 1, and the corresponding phase structures will be described in the following sections. As the number of methylene units in the side chains increases from 9 to 11, the peak maxima of the first-order transition decrease slightly. The broad endothermic event before the major first-order transition begins at around 70 °C in all three cases. However, the peak maximum of the first-order transition (91 °C) of PNBE (n = 12) is significantly lower than those of the PNBEs (n = 9−11), and the broad thermal event starts at around 60 °C. In contrast, the heats of the transitions are essentially independent of the number of methylene units (Table 1). The lack of an odd−even dependence of either the transition temperatures or the heats of the transitions on the number of methylene units in the side chains in this series with n = 9−12 is probably because the transition temperatures of laterally attached side-chain LC polymers level off at long n.[20,22,25] All of the T_g's of PNBEs (n = 9−12) are around 35−45 °C, which is similar to that of unsubstituted polynorbornene.[26]

Ordered Structures in PNBEs(n) at Room Temperature. Figure 3 shows a set of WAXD fiber patterns of the PNBEs (n = 9−12) taken at room temperature, in which the LC alignment is frozen in the glassy state. The fiber direction is parallel to the meridian direction. All of these WAXD fiber patterns have two pairs of

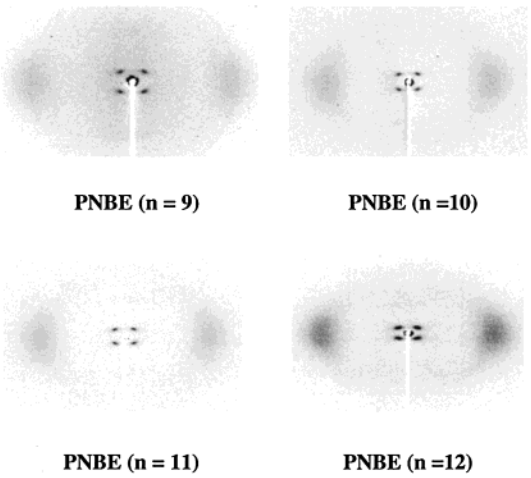

Figure 3. Set of WAXD fiber patterns of PNBEs (n = 9−12) at room temperature.

sharp low-angle reflections in the quadrants and a pair of broad scatterings on the equator. The low-angle reflection pairs in the quadrants indicate that the mesogens are organized into tilted periodic layer structures with respect to the fiber axis. The intensity and sharpness of the layer reflections gradually increase as the length of the side chains increases. However, there are apparently no second-order reflections of these layer structures, possibly because the electron density profiles normal to the layers tend to be sinusoidal, which would diminish the higher order reflections. The pair of broad scatterings on the equator demonstrates that the lateral molecular packing of both the backbones and side chains is liquidlike, with short-range order.

The WAXD results of PNBEs (n = 9−12) in Figure 3 are characteristic of a S_C phase. Although long spacers generally favor smectic mesophases in terminally attached side-chain LC polymers,[23] the S_C phase of the PNBEs (n = 9−12) with a one-carbon spacer and the N phase of the corresponding polymers with an 11-carbon spacer indicate that this may not be true in laterally attached side-chain LC polymers. However, this contradiction must be confirmed by studying the homologous series of PNBEs with a succession of spacer lengths.

Polarized FT-IR can be used to identify the group orientations of both the backbone and side chains, and therefore their relative orientation, via changes in their vibration absorption intensities. Figure 4a shows the changes in intensity of the stretching vibration of the C≡C bonds (∼2210 cm^{-1}) in the side-chain mesogens of PNBE (n = 10) at room temperature. The absorption intensity of this vibration clearly increases as the polarizer angle decreases from 90° (perpendicular to the orientation direction) to 0° (parallel to the orientation direction). This demonstrates that the mesogens in the side chains are parallel to the orientation direction. Figure 4b shows the changes in the absorption intensity of the out-of-plane bending vibration of the olefinic C−H bonds (∼970 cm^{-1}) in the backbone. The intensity of this vibration is highest at 90° and lowest at 0°, revealing that the olefinic C−H out-of-plane bending direction is oriented almost 90° to the orientation direction and that the backbones are therefore approximately parallel to the orientation direction. Both the backbone and mesogens are oriented parallel to the fiber axis at room temperature.

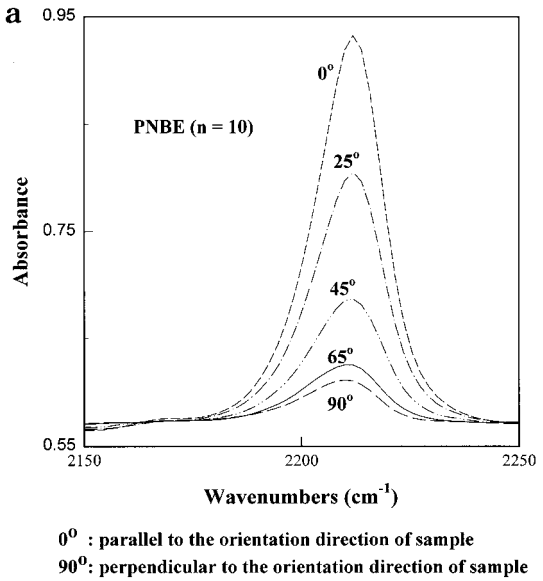

Figure 4. Two sets of polarized FTIR spectra of oriented samples of PNBE ($n = 10$) at room temperature as a function of polarizer angle with respect to the shear direction: (a) the stretching vibration of the C≡C bonds in the side chains; (b) the out-of-plane bending vibration of the ═C−H bonds in the backbone.

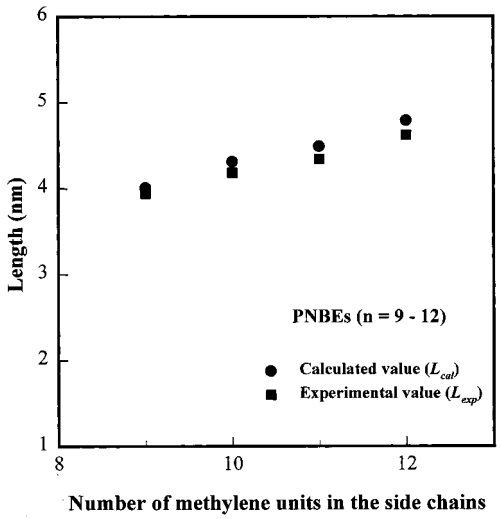

Figure 5. Side chain lengths observed experimentally and calculated from atomic lengths and bond angles for PNBEs ($n = 9-12$).

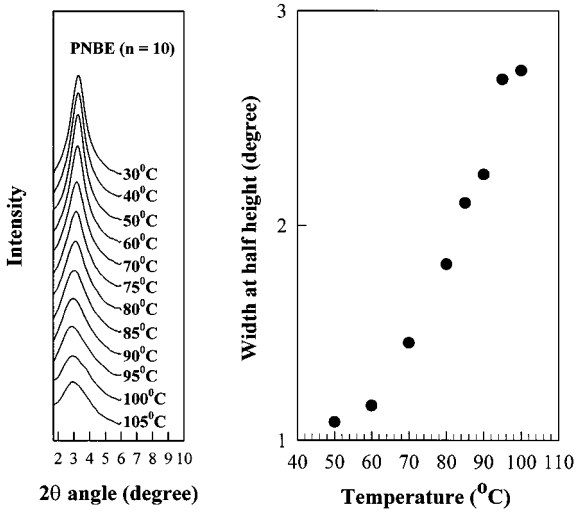

Figure 6. Changes in the low-angle WAXD reflections of the PNBE ($n = 10$) powder samples during heating. The WAHH of the low-angle reflection is also included as a function of temperature.

Figure 5 shows the length of the lateral side chains calculated by two different methods. The experimental lengths (L_{exp}) were calculated from the WAXD fiber patterns using the formula $L_{exp} = d/\cos\beta$, where d is the measured d spacing and β is the measured tilt angle of low angle reflections with respect to the meridian direction (the fiber axis), which is around 50° at room temperature. The calculated lengths (L_{cal}) were calculated using atomic bond lengths and angles, assuming that the n-alkoxy substituents are in an all-trans conformation. As shown in Figure 5, all of the L_{exp} values are slightly lower than the corresponding L_{cal} values, which indicates that the n-alkoxy substituents are not completely in an all-trans conformation.

Structural Evolution of PNBEs(n) during Heating. Figure 6 shows the WAXD powder patterns of PNBE ($n = 10$) obtained on heating, which are mirrored by WAXD powder patterns obtained on cooling. Since only one scattering halo exists in the wide-angle region and it shifts slightly to lower 2θ angles with increasing temperature due to thermal expansion, we will focus on the WAXD results in the low-angle region. The d spacing of the low-angle reflection in the WAXD powder pattern at room temperature is identical to the fiber pattern shown in Figure 3.

PNBE ($n = 10$) undergoes structural changes when it is heated above room temperature. The d spacing of the layer reflections increases significantly at the onset temperature (70 °C) of the broad transition observed by DSC. The WAHH of this reflection (Figure 6) increases with increasing temperature. Calculations using the Sherrer equation[27] demonstrate that this corresponds to a decrease in the correlation length (e.g., 11 nm at 50 °C) with increasing temperature. The change in the WAHH in Figure 6 at 95 °C corresponds to the $S_C \rightarrow N$ phase transition observed by both DSC and WAXD intensity changes (see discussion of Figure 12 below).

Figure 7 shows that the d spacings of the low-angle reflections of all four PNBEs ($n = 9-12$) increase during heating, although the increase in the d spacing of PNBE ($n = 12$) is much more pronounced and begins at a lower

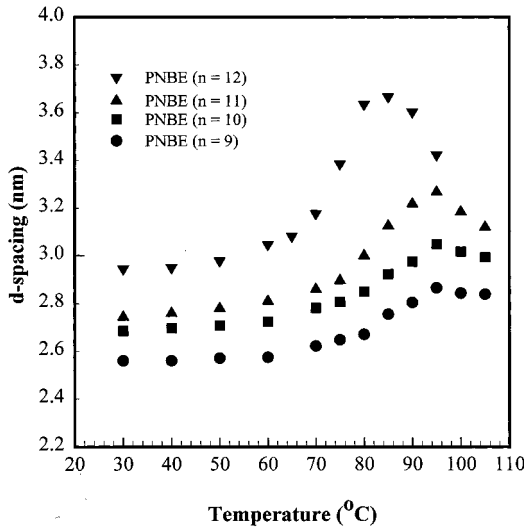

Figure 7. Changes in the *d* spacings of low-angle reflections during heating in the WAXD powder patterns of PNBEs (n = 9−12).

temperature (60 °C). This increase in the *d* spacing cannot be accounted for simply by thermal expansion and demonstrates that the tilt angle decreases during heating. After heating beyond these maxima, the *d* spacings decrease until the samples undergo isotropization, which may therefore be due to disordering of the orientation of the mesogens and/or a further disordering of the *n*-alkoxy substituents from their trans conformations. The temperature at which this decrease begins is similar in the PNBEs (n = 9−11) (95−100 °C) but significantly lower in PNBE (n = 12) (85−90 °C).

Since WAXD powder patterns lack dimensionality, we must use WAXD fiber patterns during heating to identify the phase structures in these PNBEs. Figure 8 shows a typical set of WAXD fiber patterns from PNBE (n = 10) recorded in the low-angle region at different temperatures; the pair of diffused scatterings on the equator in the wide-angle region (Figure 3) are due to the liquidlike lateral molecular packing and do not change significantly during heating and are therefore not included. With increasing temperature, the low-angle reflections gradually become diffuse, and the tilt angle between the diffraction spot and the meridian direction decreases. Above 90 °C, we can no longer determine the tilt angle precisely due to the very diffuse low-angle reflections.

Figure 9 illustrates how the tilt angles of the low-angle reflections change with heating for the PNBEs (n = 9−11). For example, the tilt angle of PNBE (n = 10) decreases slightly from 30 to 70 °C. Although DSC showed that two first-order transitions take place above 90 °C, the greatest decrease (10°) in the tilt angles occurs between 70 and 90 °C. This clearly shows that a gradual transition starts at least 28 °C below the major first-order transition(s) of PNBEs (n = 9−11) observed by DSC. Nevertheless, the PNBE (n = 10) fiber pattern in Figure 8 demonstrates that the mesogens remain tilted within the layers even at 94 °C, although the low-angle reflections are diffuse and weak, and their correlation lengths are therefore small at this temperature.

This temperature corresponds to the low-temperature first-order transition observed by DSC, which is overlapped with another high-temperature first-order transition (Figure 2), and the temperature at which the *d*

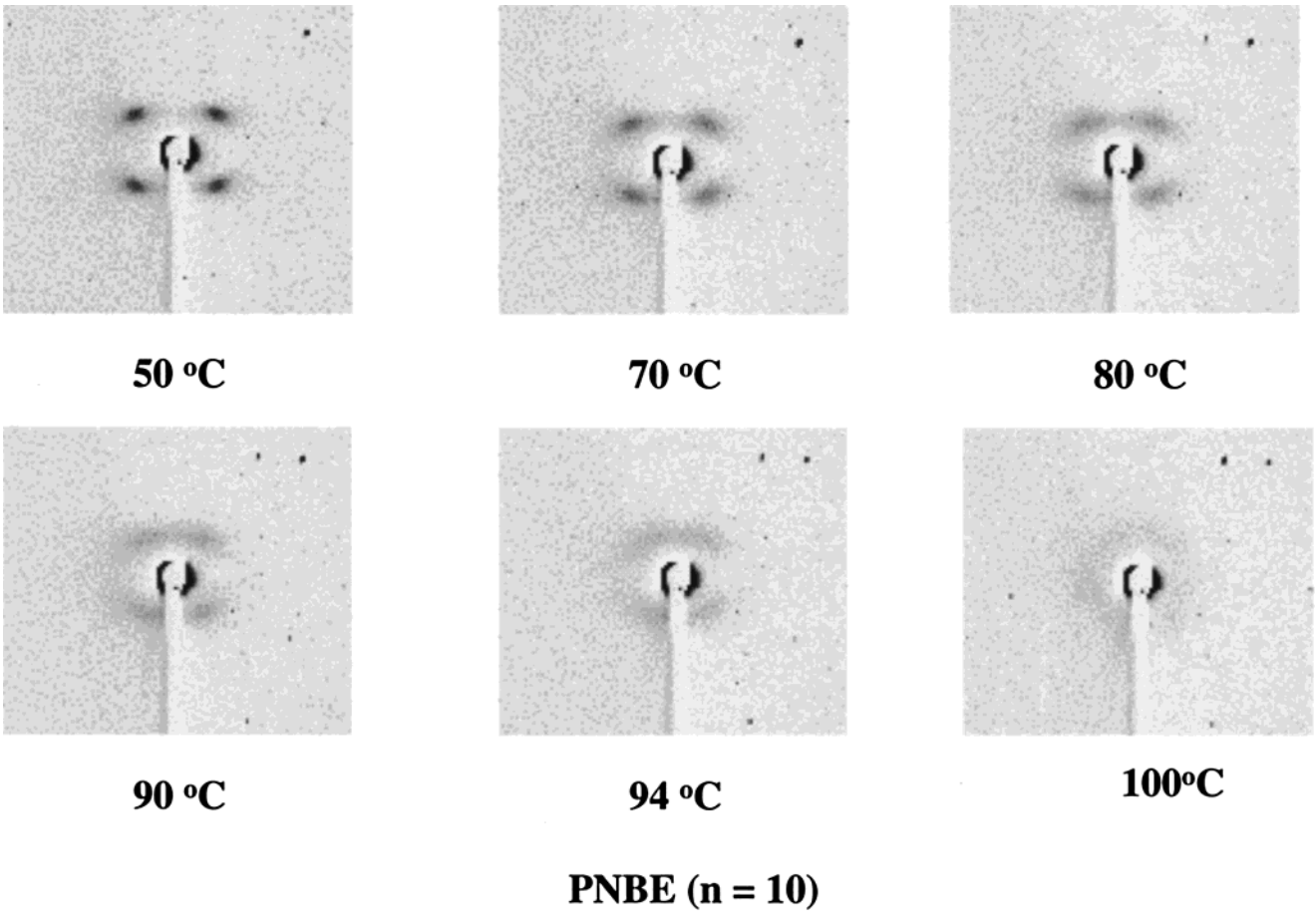

Figure 8. Set of WAXD fiber patterns in the low-angle region of PNBE (n = 10) at different temperatures.

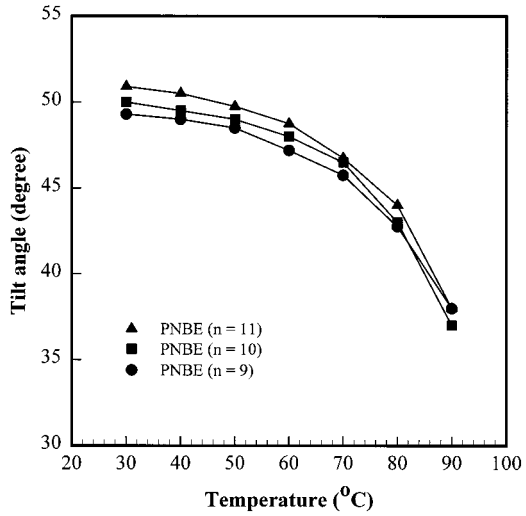

Figure 9. Changes in the tilt angle of the low angle reflections of the PNBEs (n = 9−11) with temperature.

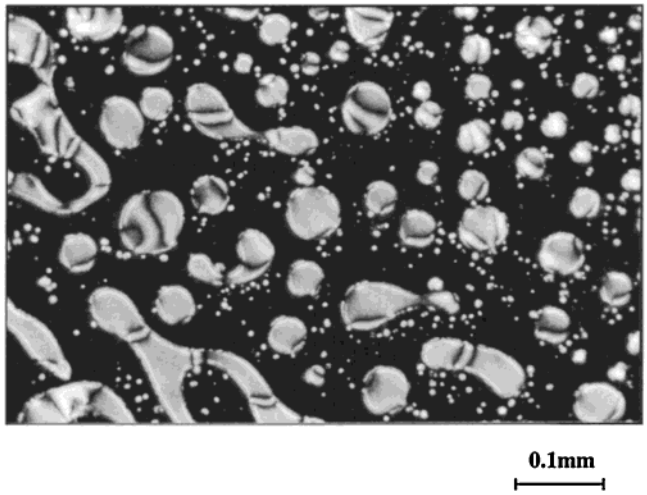

Figure 10. Nematic droplet morphology of PNBE (n = 12) observed by PLM after annealing at 89.8 °C for 11 h.

spacing of the low-angle reflection starts to decrease (Figure 7). On the other hand, Figure 10 shows a representative PLM texture of N droplets that demonstrates that all of the PNBEs (n = 9−12) organize into a N mesophase upon cooling from the isotropic melt. Figure 11 shows a representative schlieren texture of the N mesophase of PNBE (n = 10) that contains both two and four brushes and is similar to the schlieren textures exhibited by the other PNBEs reported here in the N phase. The PNBEs (n = 9−12) exhibit only a four-brush schlieren texture in the S_C phase. Therefore, the lower-temperature first-order transition observed on heating the PNBEs (n = 9−11) is a $S_C \rightarrow N$ phase transition, and the higher-temperature first-order transition of all of the PNBEs (n = 9−12) is the disordering from the N phase to the isotropic melt (I).

A S_C phase can be distinguished from a S_C fluctuation by plotting the scattering intensity as a function of temperature.[28] Figure 12 shows the corrected scattering intensity obtained from the WAXD powder patterns of PNBE (n = 10) during heating; this relationship is identical to the data obtained on cooling. The intensity at the Bragg 2θ angle decreases with increasing temperature over the temperature region where the S_C phase exists and is especially drastic between 87 and

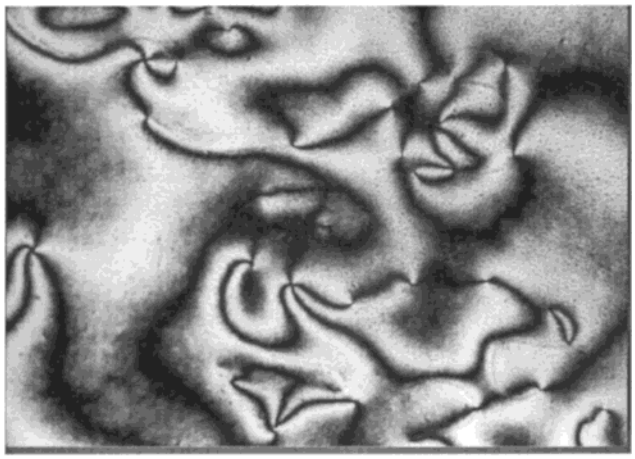

Figure 11. Schlieren nematic texture of PNBE (n = 10) observed by PLM after annealing at 96.6 °C for 5 h.

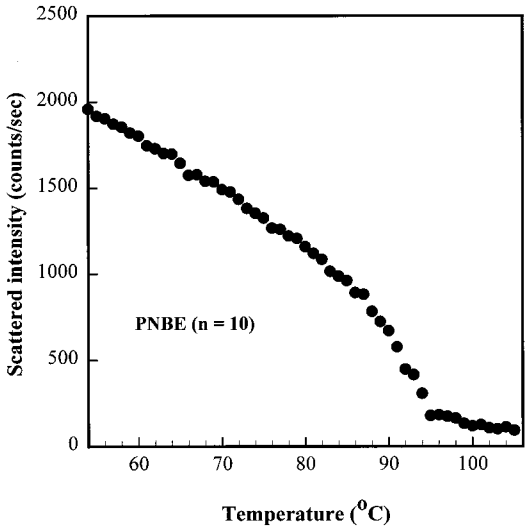

Figure 12. Measured scattering intensity versus temperature at the Bragg 2θ angle obtained from WAXD powder patterns of PNBE (n = 10).

95 °C, which corresponds to the $S_C \rightarrow N$ phase transition. Although the intensity of this Bragg angle is weak in the N phase region, there is a small but detectable decrease in the peak intensity at 99 °C. This corresponds to the $N \rightarrow I$ transition. Therefore, Figure 12 indicates that PNBE (n = 10) undergoes a true $S_C \rightarrow N$ phase transition.

Since the tilt angle is an order parameter used to distinguish between first- and second-order transitions,[29] the gradual change in the tilt angle that corresponds to the broad endothermic event observed on heating (Figure 1) should be identified as a phase transition. The transition temperature is the temperature at which the tilt angle reaches 0°. For example, the transition from a S_C to a S_A phase is second-order in low-molecular-mass liquid crystals if the tilt angle in the S_C phase decreases continuously and finally reaches 0°. If the decrease is discontinuous with a sudden drop to 0°, the transition is first-order.[29−31] Although the tilt angles in the PNBEs (n = 9−11) decrease continuously above 70 °C, the S_C phase of the PNBEs (n = 9−11) transforms via a first-order transition to a N phase before the tilt angle reaches 0°. The

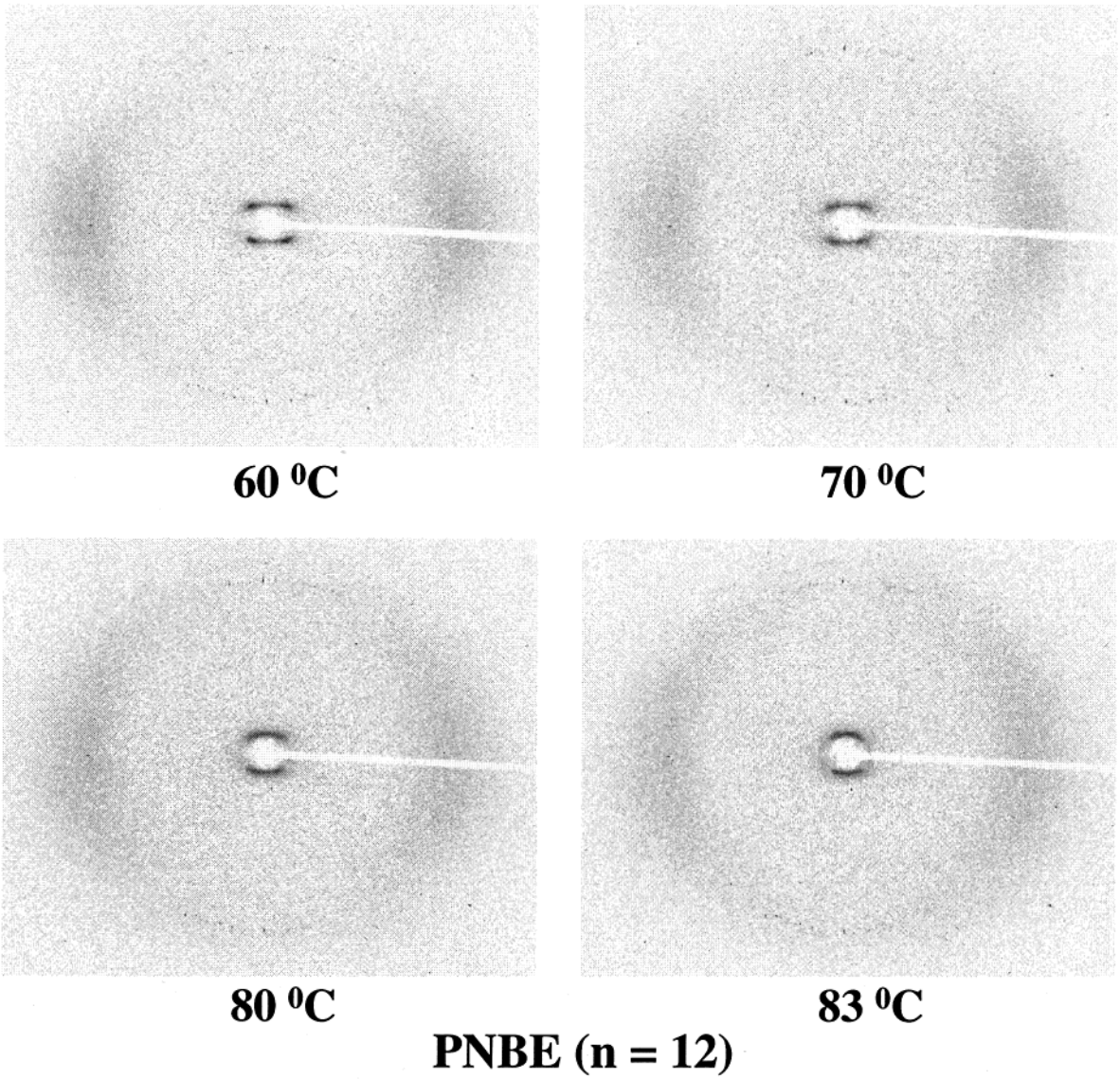

Figure 13. Set of WAXD fiber patterns of PNBE ($n = 12$) at different temperatures during heating.

S_A phase is not experimentally accessed in the LC phase transitions of these PNBEs ($n = 9-11$).

However, increasing the length of the *n*-alkoxy substituents to 12 methylenic units apparently stabilizes the S_A phase. Figure 13 shows the WAXD fiber patterns for PNBE ($n = 12$) during heating. (As shown in Figure 3, there are two pairs of strong low-angle reflections in the quadrants at room temperature.) With increasing temperature, the tilt angle between the low-angle reflections and the meridian direction gradually decreases until there is a typical S_A WAXD fiber pattern with only one pair of strong low-angle reflections on the meridian at temperatures above 83 °C. Therefore, PNBE ($n = 12$) clearly undergoes a $S_C \rightarrow S_A$ phase transition.

Figure 14 shows that the tilt angle of the S_C phase of PNBE ($n = 12$) decreases to 0° at around 85 °C. The corresponding azimuthal intensity profiles inserted into this figure confirm that the change in this tilt angle is continuous. The low-angle reflections in the WAXD powder patterns of PNBE ($n = 12$) in Figure 15 also continuously decrease with heating toward a larger *d* spacing. This corresponds to a gradual transition from the S_C to the S_A phase; the *d* spacing corresponds to the layer thickness of the S_A phase at 85 °C. On the other hand, the WAHH decreases with increasing temperature, similar to the case shown in Figure 6. As discussed previously, therefore, although there are no first-order transition peaks in this temperature region of the DSC cooling and heating diagrams, there is a broad thermal event with a gradual change in the heat capacity. Therefore, the $S_C \leftrightarrow S_A$ transformation is a second-order transition.[29]

The measured scattering intensity versus temperature at the low Bragg angle obtained from WAXD powder patterns of PNBE ($n = 12$) is shown in Figure 16. The intensity at this 2θ angle decreases with increasing temperature over the temperature range of the S_C phase, with a drastic drop in the intensity between 80 and 85 °C, which corresponds to a $S_C \rightarrow S_A$ phase transition. There is another drastic drop in the intensity above 85 °C, which corresponds to a $S_A \rightarrow N$ phase transition. Therefore, the two higher-temperature first-order transitions correspond to the $S_A \rightarrow N$ and the $N \rightarrow I$ phase transitions, respectively.

Conclusion

In summary, the wide-angle X-ray diffraction experiments described in this paper demonstrate that the S_C

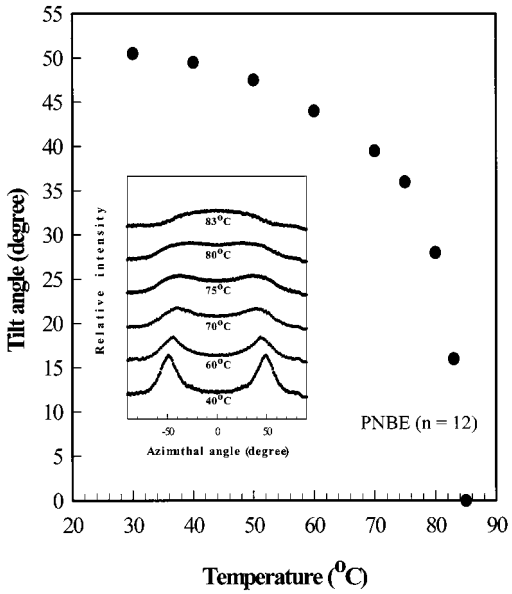

Figure 14. Changes in the tilt angle during the $S_C \rightarrow S_A$ phase transformation of PNBE ($n = 12$) as a function of temperature. Azimuthal intensity profiles of the low-angle WAXD reflections while heating the fibers are also inserted.

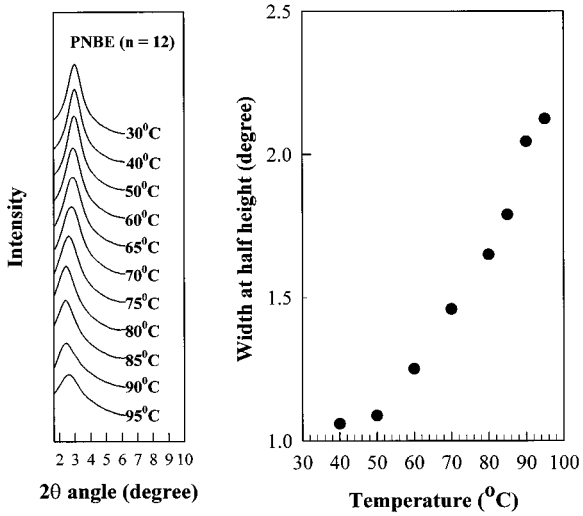

Figure 15. Changes in the low-angle WAXD reflections of PNBE ($n = 12$) powder samples during heating. The WAHH of the low-angle reflection is also included as a function of temperature.

phase can be achieved in laterally attached side-chain LC polymers by using symmetrically disubstituted extended mesogens whose low-molecular-mass analogues also exhibit the S_C phase.[1,4] All of the PNBEs ($n = 9-12$) exhibit three transitions during heating: a broad transition starting at 70 °C for PNBEs ($n = 9-11$) and 60 °C for PNBE ($n = 12$) and two overlapped first-order transitions above 90 °C for PNBEs ($n = 9-11$) and near 90 °C for PNBE ($n = 12$). The highest temperature transition corresponds to a $N \rightarrow I$ transformation. All of the polymers also possess a S_C phase at room temperature, whose tilt angle gradually decreases during heating. When the tilt angle reaches 0° in PNBE ($n = 12$), the polymer exhibits a S_A phase. The phase transformation between the S_C and the S_A phases occurs between 60 and 83 °C and is characterized by a second-order transition. Although the PNBEs ($n = 9-11$) also exhibit both the broad DSC transition starting at 70 °C, and the corresponding tilt angle changes by WAXD, the

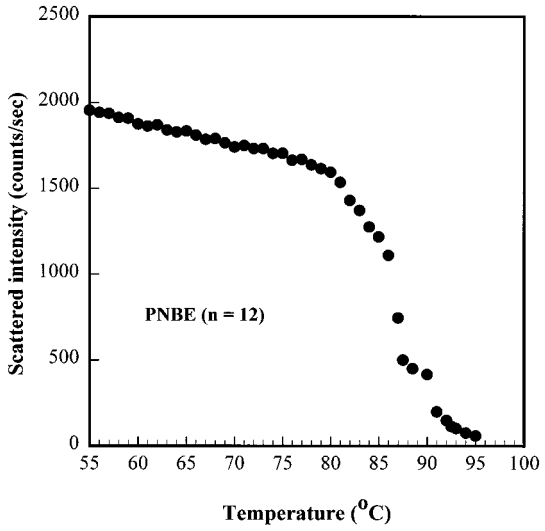

Figure 16. Measured scattering intensity versus temperature at the Bragg 2θ angle obtained from WAXD powder patterns of PNBE ($n = 12$).

transformation from the S_C to the S_A phase is not completed before these polymers undergo a first-order transition to the N phase. Therefore, the S_A phase is not experimentally observed in PNBEs ($n = 9-11$).

Acknowledgment. This work was supported by the NSF (DMR-9617030 and DMR-9996334), NSF ALCOM Science and Technology Center (DMR-8920147), and the Petroleum Research Fund, administered by the American Chemical Society.

References and Notes

(1) Pugh, C.; Liu, H.; Arehart, S. V.; Narayanan, R. *Macromol. Symp.* **1995**, *98*, 293.
(2) Le Barney, P.; Dubois, J. C. In *Side Chain Liquid Crystal Polymers*; McArdle, C. B., Ed.; Chapman and Hall: New York, 1989; Chapter 5.
(3) Demus, D.; Zaschke, H. *Flussige Kristalle in Tabellen II*; VEB Deutscher Verlag: Leipzig, 1984.
(4) Pugh, C.; Arehart, S. V.; Liu, H.; Narayanan, R. *J. Macromol. Sci., Pure Appl. Chem.* **1994**, *A31*, 1591.
(5) See for example: (a) Campillos, E.; Marcos, M.; Serrano, J. L.; Alonso, P. J.; Martinez, J. I. *J. Mater. Chem.* **1996**, *6*, 533. (b) Thomas, E. L.; Chen, J. T.; Orourke, M. J. E.; Ober, C. K.; Mao G. P. *Macromol. Symp.* **1997**, *117*, 241. (c) Deschenaux, R.; Jauslin, I.; Scholten, U.; Turpin, F.; Guillon, D.; Heinrich, B. *Macromolecules* **1998**, *31*, 5647. (d) Gallot, B.; Galli, G.; Ceccanti, A.; Chiellini, E. *Polymer* **1999**, *40*, 2561.
(6) Hessel, F.; Finkelmann, H. *Polym. Bull.* **1985**, *14*, 375.
(7) Hessel, F.; Herr, R. P.; Finkelmann, H. *Makromol. Chem.* **1987**, *188*, 1597.
(8) Zhou, Q. F.; Li, H. M.; Feng, X. D. *Macromolecules* **1987**, *20*, 233.
(9) Zhou, Q. F.; Li, H. M.; Feng, X. D. *Mol. Cryst. Liq. Cryst.* **1988**, *155*, 73.
(10) Hardouin, F.; Mery, S.; Achard, M. F.; Mauzac, M.; Davidson, P.; Keller, P. *Liq. Cryst.* **1990**, *8*, 565.
(11) Leube, H. F.; Finkelmann, H. *Makromol. Chem.* **1990**, *191*, 2707.
(12) Leube, H. F.; Finkelmann, H. *Makromol. Chem.* **1991**, *192*, 1317.
(13) Hardouin, F.; Mery, S.; Achard, M. F.; Noirez, L.; Keller, P. *J. Phys. II* **1991**, *1*, 511 and 871 (Erratum).
(14) Lewthwaite, R. A.; Gray, G. W.; Toyne, K. J. *J. Mater. Chem.* **1992**, *2*, 119.
(15) Hardouin, F.; Leroux, N.; Mery, S.; Noirez, L. *J. Phys. II* **1992**, *2*, 271.
(16) Percec, V.; Tomazos, D. *J. Mater. Chem.* **1993**, *3*, 643.
(17) Leroux, N.; Keller, P.; Achard, M. F.; Noirez, L.; Hardouin, F. *J. Phys. II* **1993**, *3*, 1289.
(18) Arehart, S. V.; Pugh, C. *J. Am. Chem. Soc.* **1997**, *119*, 3027.

(19) Pugh, C.; Bae, J.-Y.; Dharia, J.; Ge, J. J.; Cheng, S. Z. D. *Macromolecules* **1998**, *31*, 5188.
(20) Pugh, C.; Shao, J.; Ge, J. J.; Cheng, S. Z. D. *Macromolecules* **1998**, *31*, 1779.
(21) Pugh, C.; Andersson, S. K.; Percec, V. *Liq. Cryst.* **1991**, *10*, 229.
(22) Pugh, C.; Dharia, J.; Arehart, S. V. *Macromolecules* **1997**, *30*, 4520.
(23) (a) Pugh, C.; Kiste, A. L. *Prog. Polym. Sci.* **1997**, *22*, 601. (b) Pugh, C.; Kiste, A. L. In *Handbook of Liquid Crystals*; Demus, D., Goodby, J. W., Gray, G. W., Spiess, H. W., Vill, V., Eds.; VCH: Weinheim, 1998; Vol. 3, Chapter 3.
(24) Ge, J. J.; Honigfort, P. S.; Ho, R.-M.; Wang, S.-Y.; Harris, F. W.; Cheng, S. Z. D. *Macromol. Chem. Phys.* **1999**, *200*, 31.
(25) Pugh, C.; Schrock, R. R. *Macromolecules* **1992**, *25*, 6593.
(26) Komiya, Z.; Schrock, R. R. *Macromolecules* **1993**, *26*, 1387.
(27) Kakudo, M.; Kasai, N. *X-ray Diffraction by Polymers*; Elsevier: New York, 1972; p 329.
(28) McMillan, W. L. *Phys. Rev. A* **1972**, *6*, 936.
(29) Clark, N. A.; Lagerwall, S. T. In *Ferroelectric Liquid Crystals*; Goodby, J. W., Ed.; Gordon and Breach Science Publishers: Philadelphia, 1991; Chapter 1.
(30) Dumrongrattana, S.; Huang, C. C. *Phys. Rev. Lett.* **1986**, *56*, 464.
(31) Isogai, M.; Kondo, K.; Kitazumi, T.; Mukoh, A.; Nagae, Y.; Kawakami, H. *Jpn Display '86* **1986**, 472.

MA9918607